Chemosphere 325 (2023) 138360

Contents lists available at ScienceDirect

Chemosphere

journal homepage: www.elsevier.com/locate/chemosphere

Hazard assessment of different-sized polystyrene nanoplastics in hematopoietic human cell lines

Alireza Tavakolpournegari [a,1], Balasubramanyam Annangi [a,1], Aliro Villacorta [a,b], Gooya Banaei [a], Joan Martin [a], Susana Pastor [a], Ricard Marcos [a,*,1], Alba Hernández [a,1,**]

[a] Group of Mutagenesis, Department of Genetics and Microbiology, Faculty of Biosciences, Universitat Autònoma de Barcelona, Cerdanyola Del Vallès, Barcelona, Spain
[b] Facultad de Recursos Naturales Renovables, Universidad Arturo Prat, Iquique, Chile

HIGHLIGHTS

- Polystyrene nanoplastics were evaluated in Raji-B, THP-1, and TK6 cells.
- TEM, confocal microscopy, and flow cytometry demonstrated cell internalization.
- Cell uptake was negatively associated with the size.
- Mitochondrial membrane potential loss was induced in Raji-B and THP-1 cells.
- Size, biological endpoint, and cell type modulate the toxicological profile of MNPLs.

GRAPHICAL ABSTRACT

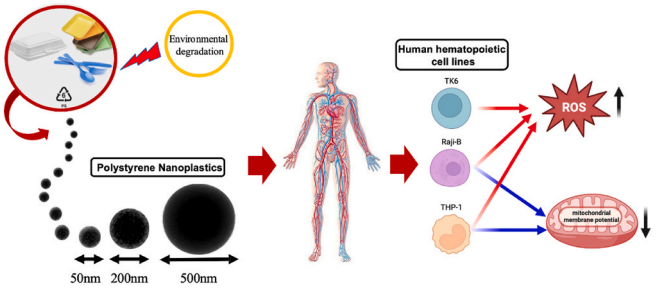

ARTICLE INFO

Handling Editor: Michael Bank

Keywords:
Polystyrene nanoplastic size
Raji-B/THP-1/TK6 cells
Uptake
Oxidative stress
Mitochondrial membrane potential

ABSTRACT

The environmental presence of micro/nanoplastics (MNPLs) is an environmental and human health concern. Such MNPLs can result from the physicochemical/biological degradation of plastic goods (secondary MNPLs) or can result from industrial production at that size, for different commercial purposes (primary MNPLs). Independently of their origin, the toxicological profile of MNPLs can be modulated by their size, as well as by the ability of cells/organisms to internalize them. To get more information on these topics we have determined the ability of three different sizes of polystyrene MNPLs (50, 200, and 500 nm) to produce different biological effects in three different human hematopoietic cell lines (Raji-B, THP-1, and TK6). Results show that none of the three sizes was able to induce toxicity (growth ability) in any of the tested cell types. Although transmission electron microscopy and confocal images showed cell internalization in all the cases, their quantification by flow cytometry demonstrated an important uptake by Raji-B and THP-1 cells, in comparison with TK6 cells. For the first ones, the uptake was negatively associated with the size. Interestingly, when the loss of mitochondrial membrane potential was determined, dose-related effects were observed for Raji-B and THP-1 cells, but not for TK6 cells. These effects were observed for the three different sizes. Finally, when oxidative stress induction was evaluated, no clear effects were observed for the different tested combinations. Our conclusion is that size, biological endpoint, and cell type are aspects modulating the toxicological profile of MNPLs.

* Corresponding author. Group of Mutagenesis, Department of Genetics and Microbiology, Faculty of Biosciences, Universitat Autònoma de Barcelona, Campus of Bellaterra, 08193, Cerdanyola Del Vallès, Spain.
** Corresponding author.
E-mail addresses: ricard.marcos@uab.cat (R. Marcos), alba.hernandez@uab.cat (A. Hernández).
[1] Both authors contribute equally.

https://doi.org/10.1016/j.chemosphere.2023.138360
Received 14 January 2023; Received in revised form 25 February 2023; Accepted 8 March 2023
Available online 10 March 2023

1. Introduction

Environmental plastic waste constitutes a serious ecological problem since they degrade slowly and remain in the environment for hundreds of years (Kik et al., 2020). In addition, these environmental plastics further degrade into micro/nanoplastics (MNPLs). Fragmented or otherwise miniaturized plastic materials in the form of MNPLs are of nagging environmental concern. Since the ubiquitous presence of MNPLs in the environment is inevitable, they can be internalized by any kind of organism, including humans. Thus, the assessment of MNPLs as potential health risk factors for humans demands an urgent response (Yong et al., 2020; Rubio et al., 2020a; Mamun et al., 2023).

Environmental plastic waste differs in its chemical composition. Approximately 90% of the total amount of plastics consists of high-density polyethylene, low-density polyethylene, polyvinyl chloride, polystyrene, polypropylene, and polyethylene terephthalate (Tursi et al., 2022). Consequently, it is assumed that environmental pollutants MNPLs are representative of these proportions. One of the main plastics used for packaging, commercial, and construction purposes is polystyrene (PS) (Kik et al., 2020). In addition, pristine PSMNPL beads are also used in the production of cosmetics (Xu et al., 2020). Environmental PSMNPLs, either because of plastic degradation goods (secondary MNPLs) or as produced at that size for different industrial purposes (primary MNPLs), enter the exposed organism inducing a wide range of hazardous effects (Qiao et al., 2022). Ingestion is considered the main way of entry of PSMNPLs into the human body. Using *in vitro* models of the intestinal barriers PSNPLs have shown their ability to translocate the barrier and affect lymphocytic cells placed after the intestinal barrier (Domenech et al., 2020). This supposes that once internalized, PSNPLs can interact with blood cell components (as a first instance), later reaching other organs and tissues. Consequently, hematopoietic cells are considered a target of PSNPLs exposure.

The potential toxic effects of PSNPLs may change by various factors, including size and surface charge. In general, it is assumed that small size and positive charge favor cell internalization and hazardous effects (Halimu et al., 2022). Nevertheless, the effect of surface charge is ambiguous, with negatively charged PSNPLs inducing a higher agglomeration modulating the toxic effects in ascidians (Eliso et al., 2020). Furthermore, positively charged PSMNPLs were more toxic on human nasal epithelial cells than negatively charged ones (Huang et al., 2022). Regarding the size effect, it is assumed that smaller sizes can easily be internalized by cells and cross biological barriers (Ramsperger et al., 2022). Nevertheless, *in vivo* results are contradictory. Thus, in the white-leg shrimp, although small PS sizes were more bioavailable and exhibited greater damage in the guts and gills, larger sizes increased the biomarkers of oxidative stress and altered microbiota components (Zhou et al., 2023). In zebrafish, larvae exposed to high-density polyethylene showed that small size caused morphological changes in the gastrointestinal cells while larger size damaged the mechanosensory receptors in the fish's lateral line system (Kim et al., 2022). Especially relevant is the study carried out in mice with two different-sized polyethylene MPLs testing different parameters detecting intestinal function (gene expression related to epithelial, permeability, and inflammatory biomarkers) where the most marked deleterious effects were found after co-exposure with the two sizes (Djouina et al., 2022).

Aiming to determine the role of MNPL size on their potentially hazardous effects, we have assessed the toxic effects of different sizes of PSNPLs (50, 200, and 500 nm). Since the blood compartment is considered the first target, once MNPLs have crossed the biological barriers, blood cells were selected. Thus, three different human hematopoietic cell types such as Raji-B (as a B-lymphocyte model), THP-1 (as a macrophage model), and TK6 (as a lymphoblastoid model) were used. Cell viability, cellular uptake, intracellular ROS generation, and mitochondrial dysfunction were the evaluated effects.

2. Materials and methods

2.1. Characterization of the used PSNPLs

Three different sizes of pristine polystyrene nanoplastics were purchased from Spherotech Inc. (Chicago, USA). Namely, PSNPLs 50 nm (PS-50; PP-008-10; with nominal sizes of 0.05–0.1 μM), PSNPLs 200 nm (PS-200; PP-015-10; with nominal sizes of 0.1–0.2 μM), and PSNPLs 500 nm (PS-500; PP-05-10; with nominal sizes of 0.4–0.6 μM. All used PSNPLs were supplied as water dispersions.

For their characterization, PSNPLs dispersions were diluted to the concentration of 100 μg/mL in distilled water, or in culture medium (supplemented RPMI-1640, Biowest Inc.) supplemented with 10% fetal bovine serum (FBS), 1% glutamine, 2.5 μg/mL Plasmocin, and then analyzed by transmission electron microscopy (TEM) with a JEOL JEM-1400 instrument (JEOL LTD, Tokyo, Japan). In addition, the hydrodynamic size and the Z-potential parameters were assessed by dynamic light scattering (DLS) and laser Doppler velocimetry (LDV) methodologies, using a Malvern Zetasizer Nano ZS zen3600 device (Malvern, UK).

2.2. Labeling and detection of PSNPLs

To visualize PS-50, PS-200, and PS-500 by confocal microscopy, the particles were labeled with the commercially available textile dye *iDye Poly Pink*, from now iDye. The procedure was adapted from previously published protocols for labeling micro and nanoscale polymers (Karakolis et al., 2019; Nguyen and Tufenkji, 2022). Briefly, the steps were performed as follows. Suspensions of 1 mL of de different PSNPLs, at a final concentration of 5 mg/mL were prepared and transferred to 1.5 mL tubes, containing 0.01 g of iDye. The mixture was vigorously vortexed and transferred to a 10 mL glass tube and incubated for 2 h at 70 °C, and then cooled at room temperature. Nine mL of Milli-Q water was then added to the tube, and the suspension was centrifuged at 4000 rcf on an Amicon® Ultra-15 centrifugal Ultracel®-100 K filter 1 × 10 5 MWCO for 15 min. This step was repeated twice to remove the excess of iDye. The stained particles were stored at 4 °C protected from light until needed. To determine the labeling and fluorescence spectra, particles were examined by confocal microscopy. To such end, working suspensions at the concentration of 400 μg/mL were prepared. Two drops (20 μL) were placed on previously ethanol-washed glass slides and covered with a thin glass coverslip. The whole procedure was carried out under a laminar flow cabinet. Aggregates of particles were then analyzed using a Leica TCS SP5 confocal microscope. The excitation wavelength was set at 561 nm, and the emission spectra were collected between 585 and 700 nm. The emission was analyzed using the Leica Application Suite X 3.7.5.24914 (Leica Microsystems CMS GmbH Wetzlar, Germany). Images were collected under the same conditions, as further explained in section 2.9.

2.3. Cell culture

Human hematopoietic cell lines TK6, THP-1, and Raji-B were used for this study. All the cells were purchased from Sigma Aldrich (MO, USA). TK6 as a human lymphoblastoid cell line is one of the standard mammalian cell lines used for *in-vitro* genotoxicity/mutagenicity tests. THP-1 is a human leukemia monocytic cell line, which is extensively used to study monocyte/macrophage functions, toxicity mechanisms, signal-transduction pathways, and nutrient and drug transport. Furthermore, Raji-B is the first continuous human B lymphocyte cell line of hematopoietic origin. All the mentioned cell lines were maintained in supplemented RPMI-1640 (Biowest Inc) medium supplemented with 10% FBS, 1% glutamine, and 2.5 μg/mL Plasmocin. All cell lines were cultured at 37 °C and 5% CO_2 and, to maintain the cells, the medium was changed with fresh medium every 2–3 days.

2.4. Treatment of cells

To study the potentially toxic effects of PSNPLs, cells were exposed to the selected concentrations of PSNPLs (PS-50, PS-200, and PS-500) diluted in RMPI 1640 supplemented medium, as described in the previous section. To proceed, the density of 5×10^5 cells/mL in the volume of 200 μL were seeded on 96 well plates (1×10^5 cells/well) and exposed to the different concentrations of PSNPLs and grown for 3 h, 24 h, and 48 h, according to the experimental endpoints.

2.5. Cell viability assay

The viability of the three cell lines after exposure was measured using the Beckman counter method. After seeding cells on 96 well plates with a concentration of 5×10^5 cells/mL, they were exposed to the different concentrations of PSNPLs (0, 50, 100, 150, and 200 μg/mL) for 24 h to assess cell toxicity. After exposure, cells were diluted 1:100 to ISOTON and counted with a ZTM Series Coulter counter (Beckman Coulter Inc., CA). The obtained percentage values were calculated as the average number of the cells counted for each treatment, compared to the untreated control culture values.

2.6. Cellular uptake assessment with transmission electron microscopy (TEM)

Among the different tools to assess PSNPLs internalization, TEM was used. To such end, cells were grown in T25 cell culture flasks to reach the density of 1.7×10^6 cells/mL. Then, each flask was treated with 3 mL of a concentration of 50 μg/mL of each PSNPL, previously diluted in RMPI 1640, for 24 h. After exposure, cells were centrifuged and the pellet was fixed in 2.5% (v/v) glutaraldehyde (EM grade, Merck, Darmstadt, Germany) and 2% (w/v) paraformaldehyde (Hatfield, PA, UK) in 0.1 M cacodylate buffer (Sigma-Aldrich, Steinheim, Germany), pH 7.4. Cells were processed following conventional procedures, as previously described (Annangi et al., 2015). Briefly, samples were first post-fixed with osmium trioxide, dehydrated in acetone, later embedded in Eponate 12™ resin (Ted Pella Inc., Redding, CA), and finally polymerized at 60 °C and cut with an ultramicrotome. Ultrathin sections were placed in copper grids and contrasted with uranyl acetate and Reynolds lead citrate solutions and observed using a JEOL 1400 (JEOL LTD, Tokyo, Japan) transmission electron microscope equipped with an Erlangshen (CCD GATAN ES1000W) camera.

2.7. Cellular uptake and localization of PSNPLs analysis with confocal microscopy

The iDye-labeled PSNPLs (iDye-PSNPLs) were used to determine PSNPLs' internalization by confocal microscopy in the three selected cell lines. To this end, 80,000 cells were seeded in glass bottom microwell dishes (MatTek, Ashland, OR, USA) and exposed to iDye-PSNPLs (100 μg/mL) for 24 h. The samples were washed with PBS, and nuclei and cell membranes were stained with 1:500 Hoechst 33,342 (ThermoFisher Scientific, Carlsbad, CA, USA) and 1:500 Cellmask™ Deep Red plasma (ThermoFisher Scientific, Carlsbad, CA, USA) respectively, for 15 min at room temperature. The iDye-PSNPLs of different sizes were visualized intracellularly at emission wavelengths of 585 nm, under a Leica TCS SP5 confocal microscope. Several fields were selected randomly per sample, and the images were processed using ImageJ software having Fiji extension.

2.8. PSNPLs internalization assessment with flow cytometry

Aiming to quantify the cellular uptake of PSNPLs, flow cytometry was assessed. All three cell lines were treated for 24 h with 100 μg/mL of labeled iDye-PSNPLs. After exposure, cells were washed, collected, centrifuged, and resuspended to 7.5×10^5 cells/mL in PBS. The fluorescence inside the cells was measured by flow cytometry (CytoFlex, Beckman Coulter, USA) with excitation/emission spectra of 561/630 nm respectively. A total number of 10,000 cells were scored for all the conditions, and the data were analyzed using the Cytexpert software.

2.9. Intracellular ROS production and analysis

The production of intracellular ROS was measured by the dihydroethidium (DHE) method. The three cell lines were exposed to PSNPLs with different concentrations ranging from 0 to 50 μg/mL for 3, 24, and 48 h. After the end of the exposure time, the cells were centrifuged, pelleted, and incubated with 10 μM of DHE in PBS for 30 min at 37 °C. After DHE exposure, cells were analyzed by flow cytometry (CytoFlex, Beckman Coulter, USA). As a positive control, cells were treated with 80 μM of antimycin-A and incubated for 45 min at 37 °C. The fluorescent intensity was measured at 488–605 nm (excitation-emission spectrum) and 10,000 cells per sample were scored and analyzed with the Cytexpert software.

2.10. Mitochondrial membrane potential assay

To determine potential mitochondrial damage caused by PSNPLs in Raji-B, THP-1, and TK6 cells, the mitochondrial membrane potential assay was utilized (MitoProb TMRM assay kit, Thermofisher Scientific, USA). The cells were seeded in 96 well plates with a concentration of 5×10^5 cells/mL and exposed to all sizes of PSNPLs with concentrations (0, 50, and 100 μg/mL) lasting for 24 h. After exposure, the cells were washed twice with PBS and then they were centrifuged and the pellet obtained was resuspended in PBS. The fluorescence intensity was measured by flow cytometry (CytoFlex, Beckman Coulter, USA) with the excitation/emission of 561/585 nm, respectively. For each concentration, the total number of 10.000 cells was scored and data was analyzed by the Cytexpert software.

2.11. Statistical analysis

All data resulted from the average of three independent experiments, including duplicates of each one of them. Data were analyzed using GraphPad Prism 7 software, and the statistical analysis was performed using the two-way ANOVA with Tukey's multiple comparison test unless stated otherwise. Statistical significance was defined as a $^*P \leq 0.05$, $^{**}P \leq 0.01$, $^{***}P \leq 0.001$.

3. Results and discussion

3.1. Characterization and dispersion of PSNPLs

The present study determined the average size and shape of the supplied pristine PSNPLs, with nominal sizes of 100–200, 400–600, and 400–900 nm by using TEM. The obtained average sizes for PS-50, PS-200, and PS-500 wetted in distilled H_2O, or in supplemented RPMI-1640 medium, are indicated in Fig. 1. In general, they are in accordance with the manufactured specified range of sizes. Furthermore, all the shapes of the used PSNPLs were spherical, both in distilled H_2O and in supplemented RPMI-1640. Table 1 shows the hydrodynamic radius (or mean size diameter) determined with a Zetasizer Nano ZS device, both in distilled H_2O and in supplemented RPMI-1640. It is important to point out the protein corona generated when dispersed in the culture medium, and the tendency to agglomerate when dispersed in supplemented RPMI-1640 over water dispersion. Moreover, the measurement of the Z-potential in supplemented RPMI-1640 revealed less stability, as reflected by the lower Zeta values when compared to PSNPLs dispersed in H_2O. Finally, the polydispersity index (PDI) values were close to zero suggesting they were monodispersed.

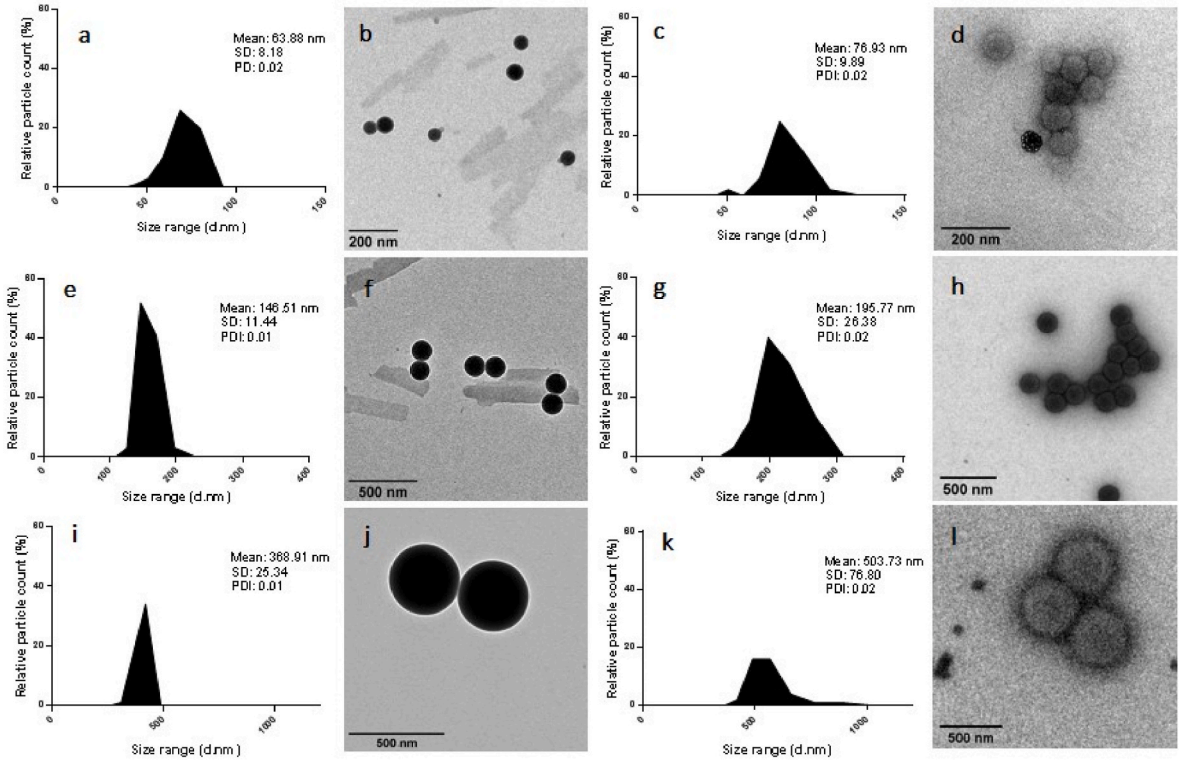

Fig. 1. The graphs indicate the size distribution (mean ± SD) and polydispersity index in water and in supplemented RPMI-1640, of PS-50 (a, c); PS-200 (e, g); and PS-500 (i, k). The TEM images show round shapes in both water and in supplemented RPMI-1640 for PS-50 (b, d), PS-200 (f, h), and PS-500 (j, l).

Table 1
Characteristics of the selected PSNPLs when dispersed in water or in supplemented RPMI-1640 cell culture medium. The hydrodynamic radius or average size in diameter (Z-average), the zeta potential, and the polydispersity index (PDI) of PS-50, PS-200, and PS-500 nm are shown, Data are represented as (mean ± SD).

	Milli-Q H_2O			SUPPLEMENTED RPMI-1640		
	PS-50	PS-200	PS-500	PS-50	PS-200	PS-500
Z-average	94.00 ± 0.86	188.00 ± 2.98	488.00 ± 7.09	94.50 ± 0.39	185.00 ± 2.10	588.70 ± 5.37
PDI	0.03 ± 0.02	0.04 ± 0.03	0.03 ± 0.02	0.09 ± 0.01	0.05 ± 0.03	0.26 ± 0.13
Z-potential	−44.90 ± 0.49	−45.00 ± 0.24	−50.40 ± 0.94	−11.70 ± 3.05	−10.10 ± 1.86	−16.00 ± 0.81

3.2. Visualization and spectral analysis

PSNPLs were successfully labeled with iDye, using the previously reported method (Nguyen and Tufenkji, 2022). The colored particles were easily visualized by confocal microscopy in all three cases (Fig. 2a and b, c) and the obtained emission spectra from 585 to 700 nm are depicted at the right of each image. The peak of emission was consistently between 610 and 620 nm. On the other hand, no fluorescence was detectable for any of the not labeled PSNPLs. Interestingly, no background fluorescence was observed indicating a lack of leaching.

3.3. Cell viability

To assess the cytotoxic potential of the three different PSNPLs' sizes, TK6, THP-1, and Raji-B cells were exposed to a range of concentrations (0–200 μg/mL). The obtained results are indicated in Fig. 3. The data revealed no significant decrease in cell viability, independently of the PSNPLs size and the concentration used, after exposures lasting for 24 h. Since none of the concentrations of PSNPLs in any of the cell lines was cytotoxic, the study further utilized and tested the sub-toxic doses of PSNPLs (≤100 μg/mL) for the rest of the experiments. In agreement, the exposure of PS-50 to the same cell types (Raji-B, THP-1, and TK6) as well as in human colorectal adenocarcinoma (Caco-2) cells did not result in a

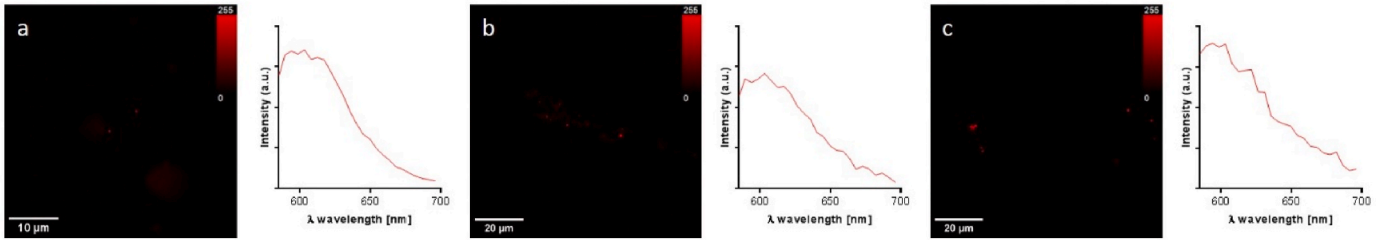

Fig. 2. Visualization of PS-50, PS-200, and PS-500 labeled with iDye Poly Pink (a, b, and c, respectively). At the right, their respective spectra are shown. (For interpretation of the references to color in this figure legend, the reader is referred to the Web version of this article.)

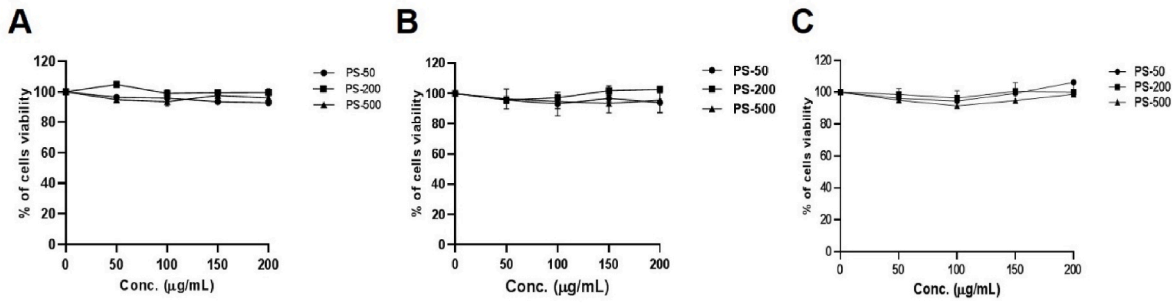

Fig. 3. Cell viability effects of different sizes and concentrations of PSNPLs in various hematopoietic cell lines. (A) The percentage of cell viability in Raji-B cells. (B) The percentage of cell viability in THP-1 cells. (C) The percentage of cell viability in TK6 cells. Exposures last for 24 h. Data are represented as (mean ± SEM).

decrease in cell viability in any of them and at various concentrations and time points (Cortés et al., 2020; Rubio et al., 2020b). Besides, PSNPLs (100 nm and 1 μm) exposure in mouse hippocampal neuronal (HT22) cells yielded a mild cytotoxic response only with the smaller sized PS-100 but not PSNPLs of 1 μm indicating a possible size effect (Liu et. al 2022). In addition, PSNPLs (20 and 70 nm) were able to reduce cell viability when used to expose human alveolar epithelial cells (A549) at different concentrations (Xu et al., 2019).

3.4. Cellular internalization of PSNPLs using different analytical tools

The assessment of cellular internalization or uptake of PSNPLs was undertaken by utilizing various analytical tools like TEM, confocal microscopy, and flow cytometry considering they could complement one another and overcome the limitations among them to provide robust information on the cellular internalization of PSNPLs.

3.5. Transmission electron microscopy (TEM)

The first approach to evaluate the cellular uptake of non-fluorescent pristine PSNPLs in the selected cell types was TEM. This technique helps to locate and visualize PSNPLs in the cell ultrastructure. The obtained TEM images demonstrated the significant internalization of the different sizes of PSNPLs (50 μg/mL, 24 h) in all the selected cell lines (Fig. 4). According to the observed micrographs, PSNPLs were found localized in or near different cellular compartments based on their size, apart from being present in the cytoplasm of the cells. TEM images showed PSNPLs incorporation in different cell organelles like mitochondria of Raji-B

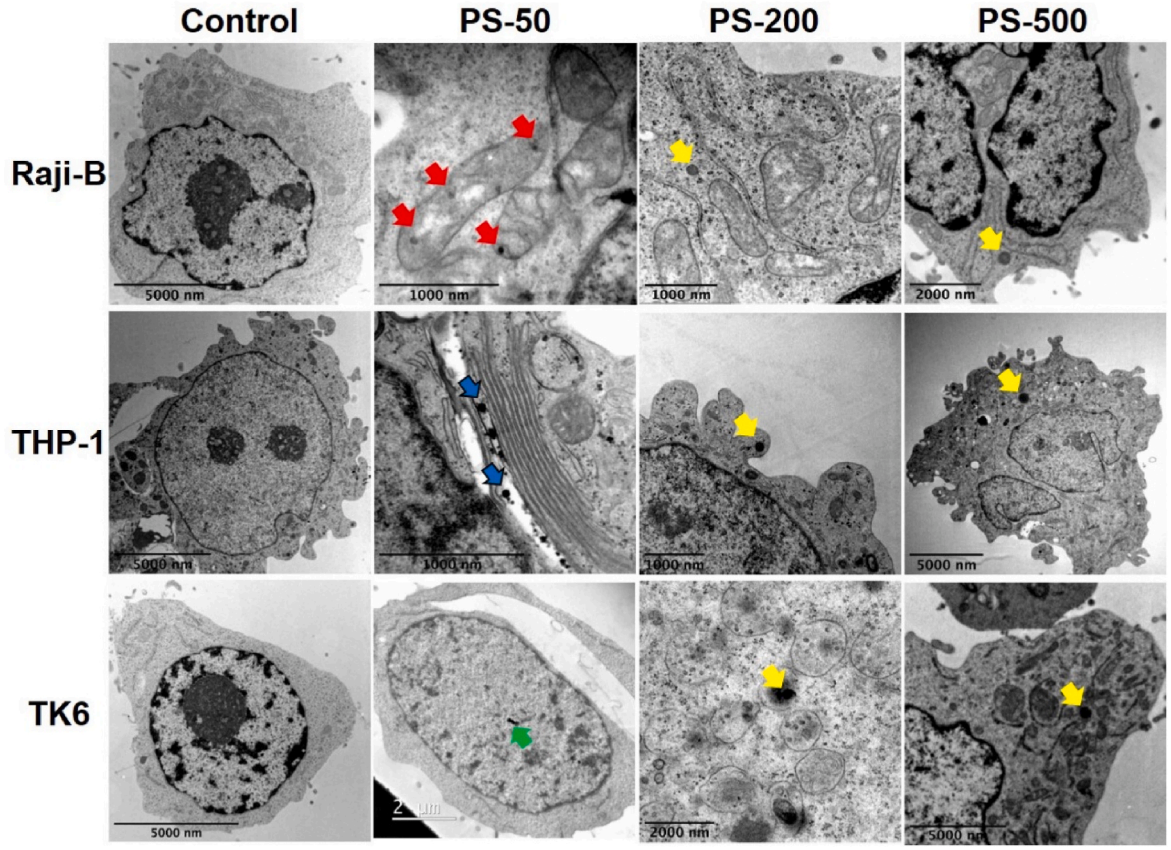

Fig. 4. Representative TEM images showing the cellular internalization and localization of the three different sizes of pristine PSNPLs in Raji-B, THP-1, and TK6 cells after treatments lasting for 24 h. Arrows in red indicate PSNPLs in mitochondria, yellow in cytoplasmic regions, green in the nucleus, and blue in the endoplasmic reticulum. (For interpretation of the references to color in this figure legend, the reader is referred to the Web version of this article.)

cells and endoplasmic reticulum of THP-1 cells. Furthermore, they were able to reach the nuclei, as observed in TK6 cells.

3.5.1. Confocal microscopy

Due to the success in staining PSNPLs (iDye-PSNPLs) they could be used in confocal microscopy. The confocal images of the treated cells revealed the significant internalization of PS-50, PS-200, and PS-500. They were mostly present in the cytoplasm and surrounding the nuclei in TK6, THP-1, and Raji-B cells after exposures lasting for 24 h (Fig. 5). Moreover, there was a size-dependent cellular internalization in all the cell lines, PS-50 being the most internalized. We assume that this elevated entry of PS-50 was due to their smaller size.

3.6. Flow cytometry

Aiming to quantify the cellular internalization of the different sizes of labeled PSNPLs flow cytometry was used. The intracellular presence of iDye-PSNPLs (100 μg/mL) in the treated cells was determined according to the fluorescence intensity, as a measure of the percentage of internalized cells. The obtained results are indicated in Fig. 6. Results indicate a cell-dependent internalization capacity according to the ranking Raji-B > THP-1 > TK6. For Raji-B and THP-1 cells, PS-50 were those showing the highest internalization, which would agree with their small size. TK6 cells showed the lowest internalization, although the detected uptake was statistically significant. This data confirms two things, such as a) cell internalization levels depend on the cell type, and b) the uptake is size dependent, showing greater internalization with the smaller size.

In the current study, the data revealed there was a size-dependent cellular internalization, PS-50 being highly internalized over PS-200 and PS-500 when studied in TEM, confocal microscopy, and flow cytometry. Moreover, we found there was a cell type-specific cellular internalization considering Raji-B was more prone to the uptake of PSNPLs followed by THP-1, and the lowest internalization by TK6 cells. In support, the cellular internalization of PS-50 was also observed in the same cell types (Raji-B, THP-1, and TK6) studied by flow cytometry (Rubio et al., 2020b). In agreement with our study, there was a size-dependent cellular internalization of PSNPLs in Caco-2 and A549 cell lines wherein PS-70 were highly internalized as compared to bigger sizes (PS-200 and PS-500), analyzed by both confocal microscopy and flow cytometry, suggesting the smaller sizes were readily accessible by the A549 and Caco-2 cells (Zhang et al., 2022). In addition, Banerjee et al. (2022) indicated that the smaller size of PSNPLs (i.e., 50 nm) was significantly internalized in HepG2 cells as compared to PS-200 and PS-500 nm, when visualized by confocal microscopy. Furthermore, it may be pointed out that the smaller size tested (i.e., PS-70 nm) would enter *via* clathrin- and caveolae-mediumted endocytosis as well as phagocytosis, while the larger particles like PS-200 and PS-500 nm could enter the A549 and Caco-2 cells only through phagocytosis and this could explain the higher internalization of the smallest NPLs (Zhang et al., 2022).

The usage of different analytical tools for cellular internalization in the present study was justified as no one tool could completely capture the NPL's internalization thoroughly due to various factors. For instance, the low atomic number of polymers in MNPLs could render them to scatter electrons weakly resulting in poor contrast under TEM (Sawyer et al., 2008). In addition, it warrants laborious sample preparation and time consumption which possibly make it irrelevant to analyze the high number of particles needed for representative studies (Ivleva, 2021). Moreover, MNPLs labeled with fluorophores could

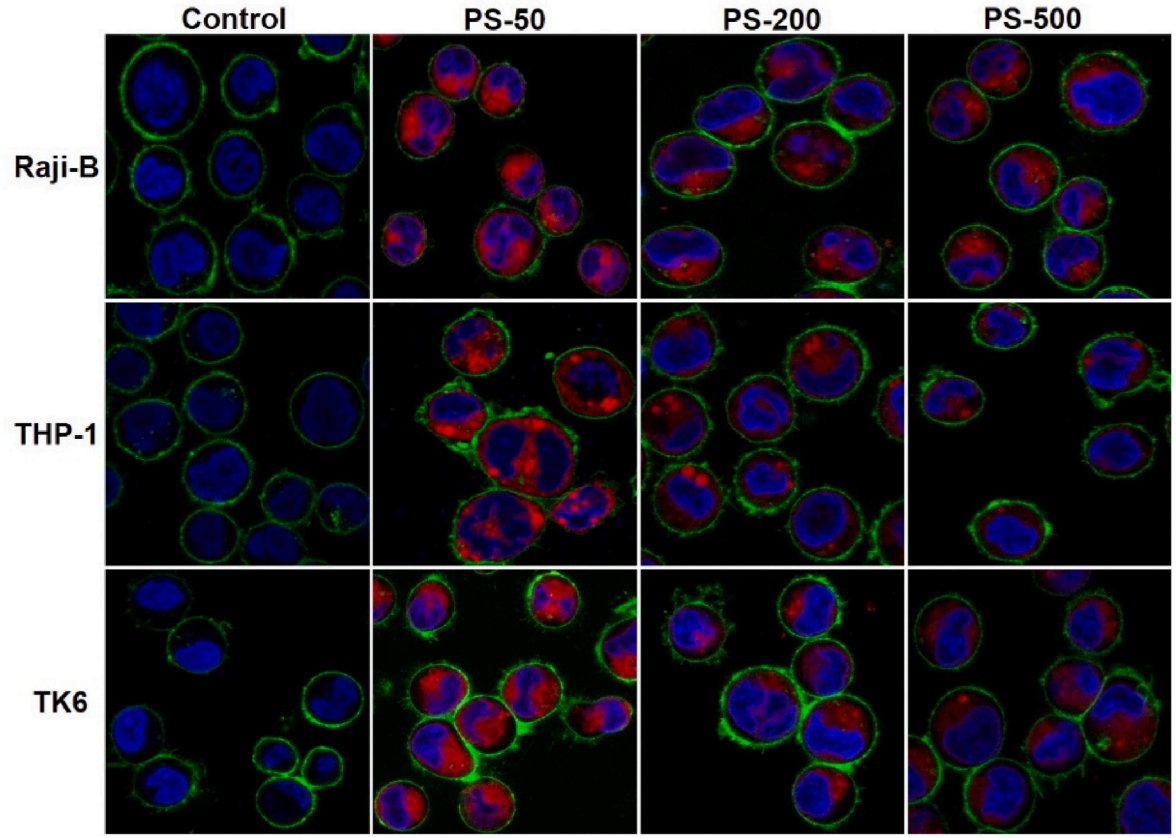

Fig. 5. Confocal microscopy images showing the cellular internalization of different sizes of iDye-PSNPLs (100 μg/mL) in Raji-B, THP-1, and TK6 cells after treatments lasting 24 h. Fluorescent iDye labeled PSNPLs are red, the cell membranes are green (cell mask), and the nuclei of the cells are blue (Hoechst 33,342). Magnification 63x. (For interpretation of the references to color in this figure legend, the reader is referred to the Web version of this article.)

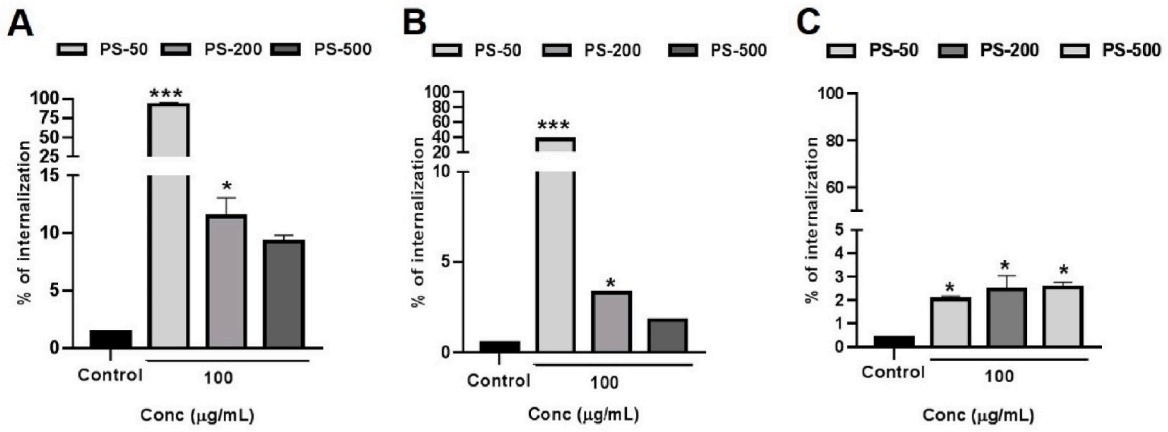

Fig. 6. Histograms showing the cell internalization of the different sizes of PSNPLs in the selected hematopoietic cells by using flow cytometry. (A) The percentage of cellular internalization in Raji-B cells, (B) in THP-1 cells, and (C) in TK6 cells. Exposures last for 24 h. Data are represented as (mean ± SEM). *$P < 0.05$, ***$P < 0.001$ (2-way ANOVA and Student's *t*-test).

possibly shed the fluorophores in cell culture medium thereby the observation of fluorescence intracellularly might be due to free fluorophores (Tenuta et al., 2011). Also, the potential leaching effect of fluorophores from the labeled PSNPLs was reported (Catarino et al., 2019). Fluorescent-labeled PSNPLs (500–1000 nm) were not able to cross the epithelial barrier of zebrafish larvae rather fluorophores alone were detected in the internal tissues. Apart, the internalization of PSNPLs could be read in flow cytometry due to an increase in the cell complexity; however, the tendency of PSNPLs to adhere to the cell surface may also reflect the increase in cell volume thereby affecting the actual estimation of their internalization in that technique (Lesniak et al., 2013; Zhang et al., 2022).

3.7. Loss of mitochondrial membrane potential

Considering the previous data showing PSNPLs' interaction with mitochondria, potential damage to these organelles was evaluated. Thus, the loss of mitochondrial membrane potential (MMP) was chosen as a biomarker of effect. Flow cytometry was used to assess the loss of MMP, using the TMRM assay, showing that entering of PSNPLs into the cells induced significant effects on the mitochondrial function, by decreasing the MMP values. Results show that all PSNPLs sizes were able to cause the loss or decrease in MMP values at the tested concentrations (50 and 100 μg/mL) in Raji-B and THP-1, cells when compared to their respective controls after 24 h ($P < 0.05$) (Fig. 7). On the other hand, TK6 cells did not show any change in MMP levels at the tested concentrations, as compared to their corresponding untreated controls after exposure to all sizes of PSNPLs for 24 h. This lack of effect could possibly be attributed to the non-interaction of PSNPLs with the mitochondria of the TK6 cells, as it was observed by TEM, where no presence of PSNPLs in or near the mitochondria of TK6 cells could be detected. Like our data on the size-dependent loss of MMP in Raji-B cells, a previous study also demonstrated the size-dependent MMP effects due to exposure of Caco-2 cells to PSMPLs sized 0.1 and 5 μm. The cells treated with 5 μm PSMPLs had a greater loss of MMP as compared to 0.1 μm sized PS (Wu et al., 2019). On the other hand, the smallest size of PSNPLs had a significant effect on the mitochondrial membrane potential in THP-1, possibly indicating a cell type-specific effect. Besides, there is no specific study comparing the size effect of PSNPLs on the mitochondrial dysfunction in THP-1 cells, our data proved relevant since the exposed THP-1 cells were more responsive to different sizes of PSNPLs, in comparison to the assessed cells like TK6. Moreover, amino-modified PSNPLs (50 nm) showed a profound effect on mitochondrial metabolic activity and in the loss of MMP in a time and dose-dependent manner, as observed in the exposed alveolar macrophages (Deville et al., 2020). Similarly, amino-modified PS-20, unmodified PS-20, and PS-50 nm caused loss of MMP, enhanced proton leak from mitochondria, as well as elevated adenosine triphosphate (ATP) generation, and mitochondrial oxidative phosphorylation in a dose-dependent way in A549 cells (Halimu et al., 2022).

3.8. Induction of intracellular reactive oxygen species (iROS)

To understand the adverse health effects of PSNPLs from a biological point of view, different biomarkers could be analyzed in human cells. One of the most important biomarkers detecting cell toxicity and cellular stress could be iROS. The role of nascent oxygen species in cell signaling under normal conditions was well established; however, their imbalance due to oxidative stress could trigger DNA damage or cellular death (Bidooki et al., 2022). Furthermore, the imbalance in the oxygen free radicals could be implicated in many debilitating diseases such as cancer-causing, cardiovascular, and neurological disorders, among others (Frijhoff et al., 2015). The assessment of the generation of iROS, by PSNPLs exposure in the different cell types, showed that there were significant size- and time-dependent increases in the percentage of iROS in all the tested cell lines. Interestingly, significantly elevated levels of iROS were found in Raji-B cells treated with larger-sized PSNPLs (e.g., PS-500; 25 μg/mL) compared to PS-50 and PS-200 nm (Fig. 8). On the other hand, PS-200 treated THP-1 (25 μg/mL) and TK6 (5–50 μg/mL) cells showed a significantly increased production of iROS (according to the results shown in Fig. 8), in comparison to PS-50 and PS-500 nm after exposures lasting for 3 h ($P < 0.05$).

Furthermore, when the exposure time was increased to 24 h, resulted in significant increases in iROS in PS-500 treated THP-1 only (10–50 μg/mL) ($P < 0.05$) (see Supplementary Fig. S1), indicating the possible time and cell-dependent transient effect. In addition, the obtained data did not indicate any increase in iROS with an increase in time up to 48 h for all sizes of PSNPLs and for all the hematopoietic cell types (see Supplementary Fig. S2).

The potential of PSNPLs to induce iROS was reported in several studies as well. Like our study, Rubio et al. (2020b) assessed the generation of iROS in the same cell types (Raji-B, THP-1, and TK6) after treating them with PS-50 at different concentrations and time points. The study demonstrated that there was a cell type-dependent induction of iROS since PS-50 (at 50 μg/mL) treated TK6 and THP-1 cells showed significant increases of iROS after 3 h, albeit there were more elevated in TK6 even after 24 h post-treatment. On the contrary, THP-1 cells were not responsive to PS-50 nm induced iROS at any of the doses and time points. Furthermore, a recent study also showed that PSNPLs could trigger iROS in a size-dependent manner in Caco-2 cells wherein the

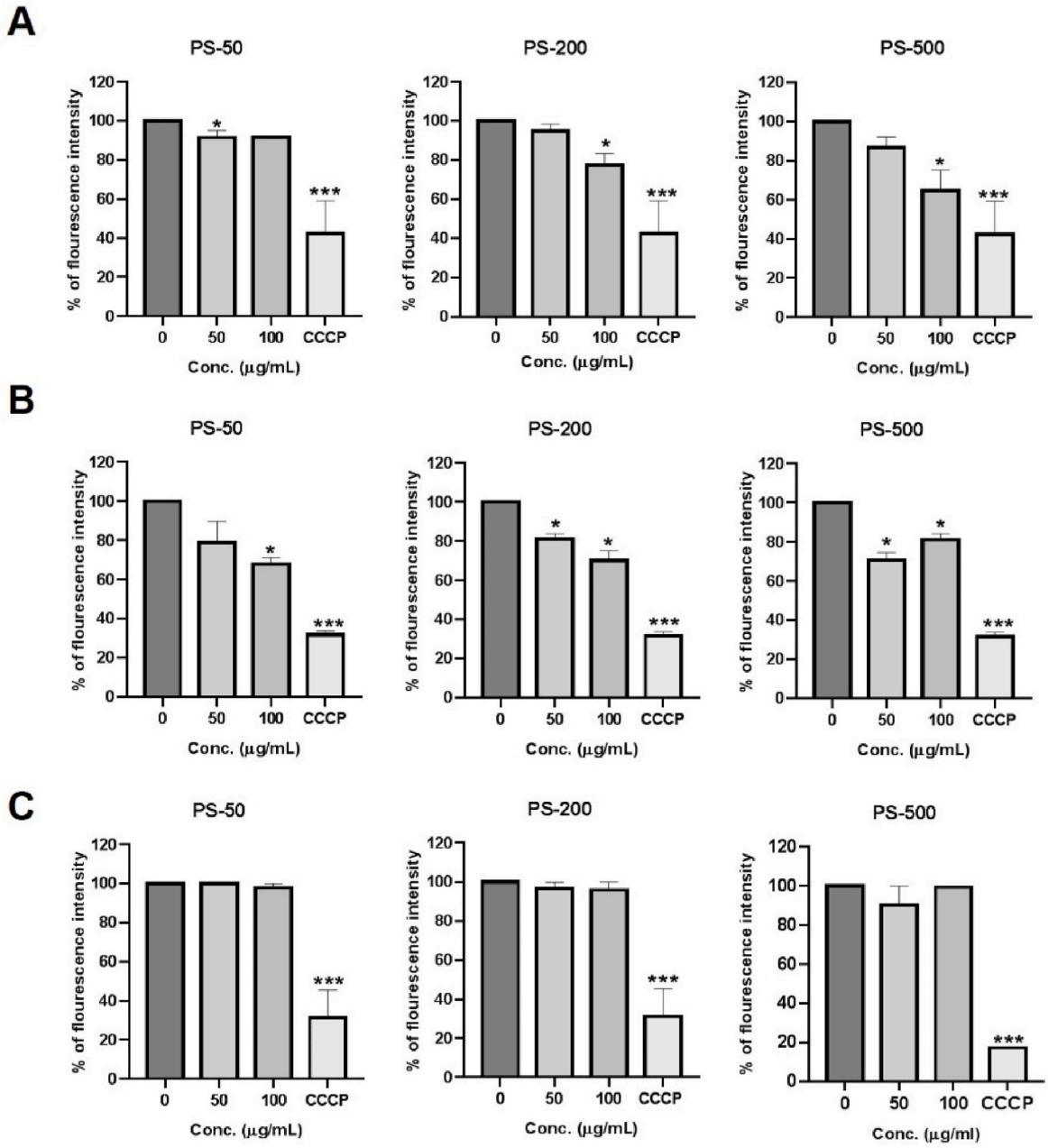

Fig. 7. The graphs indicate the loss of mitochondrial membrane potential after exposure to different sizes of PSNPLs viz. PS-50, PS-200, and PS-500 nm in Raji-B (A), THP-1 (B), and TK6 cells (C) after 24 h of treatments. Data are represented as (mean ± SEM). $^{*}P < 0.05$, $^{***}P < 0.001$ (2-way ANOVA and Student's t-test).

smaller-sized PS-300 were able to induce higher iROS, when compared to PS-500 nm and micron-sized PSNPLs (Wang et al., 2020). Similarly, PSNPLs of 40 nm were able to alter the oxidative status in the exposed human bronchiolar (BEAS-2B) and in alveolar (HPAEpiC) epithelial cells, as there were significantly elevated levels of iROS in them after 24 h, which could possibly be implicated in lung injury (Yang et al., 2021). Moreover, the surface functionalized as well as non-functionalized PSNPLS with varying sizes (amino-functionalized PS-20, non--functionalized PS-20, and PS-50 nm) triggered a dose-dependent significant increase in iROS, as well as the role of increased expression of NADPH oxidase 4 in PSNPLs induced epithelial to mesenchymal transition in A549 cells (Halimu et al., 2022). Similarly, the ability of aminated PSNPLs to induce ROS has been recently detected in murine alveolar macrophage (MH-S) cells (Wu et al., 2023). Looking for the mechanism of production of ROS and the resulting oxidative stress, and using a proteomic approach, the authors detected that the overexpression of the immunoresponsive gene 1 (*irg1*) protein was involved in the increased generation of ROS (as well of other inflammatory factors). Interestingly, and as we have observed in our study, the induction of ROS by PSNPLs has been associated with the presence of mitochondrial damage in the mouse macrophages RAW 264.7 (Chen et al., 2023). This agrees with our recent data exposing primary human nasal epithelial cells to PSNPLs, where the induction of ROS and the loss of mitochondrial membrane potential were associated with the modulation of the autophagy pathway in the form of the accumulation of LC3-II and p62, as models of autophagy markers (Annangi et al., 2023). This link between increased intracellular ROS and reduced mitochondrial membrane potential (and its consequent mitochondrial damage) has been extensively reviewed by Shadel and Horvath (2015).

In summary, it was evident that PSNPLs had the potential to induce iROS due to several contributing factors like the nature of cell type, their different sizes, doses, and surface characteristics.

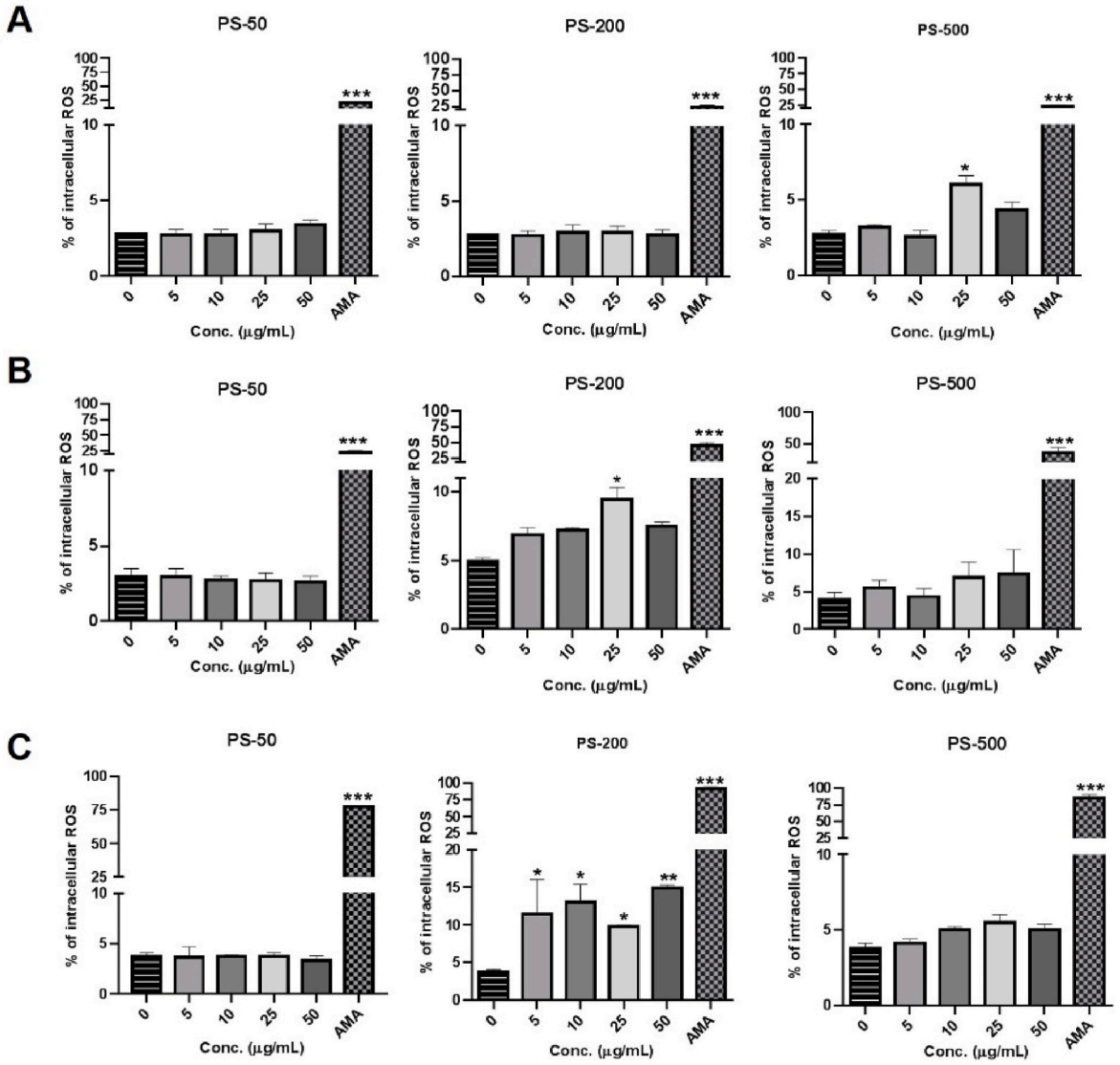

Fig. 8. The histograms show the percentage of intracellular reactive oxygen species due to exposure of different sizes of PSNPLs viz., PS-50, PS-200, and PS-500 in Raji-B (A), THP-1 (B) and TK6 cells (C) after 3 h of treatments. Data are represented as mean ± SEM. $^{*}P < 0.05$, $^{**}P < 0.01$, $^{***}P < 0.001$ (2-way ANOVA and Student's *t*-test).

4. Conclusions

The constant weathering or leaching of polymer plastics into secondary MNPLs due to various environmental factors is a major cause of concern for potential human health effects. In context, this study may provide necessary inputs for the hazard and risk assessment of MNPLs like PSNPLs when they encounter important human blood immune cell types through various routes of exposure. The release of MNPLs into the environment in various sizes and forms may need to be considered while assessing their risk. As evidenced, PSNPLs in various sizes could trigger biological responses such as cellular internalization, loss of MMP, and generation of iROS in exposed cells in a time-dependent manner. These biological responses may have cascading effects in altering or modulating the cellular functions and survival mechanisms, although they may not necessarily lead to cell death. Moreover, it is also important to understand the chronic toxic effects of PSNPLs with different sizes since there may exist a possibility of constant or continuous environmental exposure to humans.

Author contribution statement

RM and AH planned the experiments. AT, BA, AV, GB, JM, and SP carried out the experimental part. AT and BA analyzed the data, carried out the statistical analysis, prepared tables/figures, and wrote the draft manuscript. BA, RM, and AH wrote the final manuscript.

Declaration of competing interest

The authors declare that they have no known competing financial interests or personal relationships that could have appeared to influence the work reported in this paper.

Data availability

Data will be made available on request.

Acknowledgments

AT and JM hold Ph.D. FI fellowships form the Generalitat de Catalunya. AV was supported by a Ph.D. fellowship from the National

Agency for Research and Development (ANID), CONICYT PFCHA/DOCTORADO BECAS CHILE/2020–72210237. AH was granted an ICREA ACADEMIA award.

This project (Plasticheal) has received funding from the European Union's Horizon 2020 research and innovation programme under grant agreement No 965196. This work was also partially supported by the Spanish Ministry of Science and Innovation [PID 2020-116789, RB-C43] and by the Generalitat de Catalunya (2021-SGR-00731).

Appendix A. Supplementary data

Supplementary data to this article can be found online at https://doi.org/10.1016/j.chemosphere.2023.138360.

References

Annangi, B., Bach, J., Vales, G., Rubio, L., Marcos, R., Hernández, A., 2015. Long-term exposures to low doses of cobalt nanoparticles induce cell transformation enhanced by oxidative damage. Nanotoxicology 9 (2), 138–147. https://doi.org/10.3109/17435390.2014.900582.

Annangi, B., Villacorta, A., López-Mesas, M., Fuentes-Cebrian, V., Marcos, R., Hernández, A., 2023. Hazard assessment of polystyrene nanoplastics in primary human nasal epithelial cells, focusing on the autophagic effects. Biomolecules 13, 220. https://doi.org/10.3390/biom13020220.

Banerjee, S., Billey, L.O., McGarvey, A.M., Shelver, W.L., 2022. Effects of polystyrene micro/nanoplastics on liver cells based on particle size, surface functionalization, concentration, and exposure period. Sci. Total Environ. 836, 15562 https://doi.org/10.1016/j.scitotenv.2022.155621.

Bidooki, S.H., Alejo, T., Sánchez-Marco, J., Martínez-Beamonte, R., Abuobeid, R., Burillo, J.C., Lasheras, R., Sebastian, V., Rodríguez-Yoldi, M.J., Arruebo, M., Osada, J., 2022. Squalene loaded nanoparticles effectively protect hepatic AML12 cell lines against oxidative and endoplasmic reticulum stress in a TXNDC5-dependent way. Antioxidants 11, 581. https://doi.org/10.3390/antiox11030581.

Catarino, A.I., Frutos, A., Henry, T.B., 2019. Use of fluorescent-labelled nanoplastics (NPs) to demonstrate NP absorption is inconclusive without adequate controls. Sci. Total Environ. 670, 915920 https://doi.org/10.1016/j.scitotenv.2019.03.194.

Chen, J., Xu, Z., Liu, Y., Mei, A., Wang, X., Shi, Q., 2023. Cellular absorption of polystyrene nanoplastics with different surface functionalization and the toxicity to RAW264.7 macrophage cells. Ecotoxicol. Environ. Saf. 252, 114574 https://doi.org/10.1016/j.ecoenv.2023.114574.

Cortés, C., Domenech, J., Salazar, M., Pastor, S., Marcos, R., Hernández, A., 2020. Nanoplastics as a potential environmental health factor: effects of polystyrene nanoparticles on human intestinal epithelial Caco-2 cells. Environ. Sci.: Nano 7 (1), 272–285. https://doi.org/10.1039/C9EN00523D.

Deville, S., Honrath, B., Tran, Q.T.D., Fejer, G., Lambrichts, I., Nelissen, I., Dolga, A.M., Salvati, A., 2020. Time-resolved characterization of the mechanisms of toxicity induced by silica and amino-modified polystyrene on alveolar-like macrophages. Arch. Toxicol. 94 (1), 173–186. https://doi.org/10.1007/s00204-019-02604-5.

Djouina, M., Vignal, C., Dehaut, A., Caboche, S., Hirt, N., Waxin, C., Himber, C., Beury, D., Hot, D., Dubuquoy, L., Launay, D., Duflos, G., Body-Malapel, M., 2022. Oral exposure to polyethylene microplastics alters gut morphology, immune response, and microbiota composition in mice. Environ. Res. 212 (Pt B), 113230 https://doi.org/10.1016/j.envres.2022.113230.

Domenech, J., Hernández, A., Rubio, L., Marcos, R., Cortés, C., 2020. Interactions of polystyrene nanoplastics with *in vitro* models of the human intestinal barrier. Arch. Toxicol. 94 (9), 2997–3012. https://doi.org/10.1007/s00204-020-02805-3.

Eliso, M.C., Bergami, E., Manfra, L., Spagnuolo, A., Corsi, I., 2020. Toxicity of nanoplastics during the embryogenesis of the ascidian *Ciona robusta* (Phylum Chordata). Nanotoxicology 14 (10), 1415–1431. https://doi.org/10.1080/17435390.2020.1838650.

Frijhoff, J., Winyard, P.G., Zarkovic, N., Davies, S.S., Stocker, R., Cheng, D., Knight, A.R., Taylor, E.L., Oettrich, J., Ruskovska, T., Gasparovic, A.C., Cuadrado, A., Weber, D., Poulsen, H.E., Grune, T., Schmidt, H.H., Ghezzi, P., 2015. Clinical relevance of biomarkers of oxidative stress. Antioxidants Redox Signal. 23 (14), 1144–1170. https://doi.org/10.1089/ars.2015.6317.

Halimu, G., Zhang, Q., Liu, L., Zhang, Z., Wang, X., Gu, W., Zhang, B., Dai, Y., Zhang, H., Zhang, C., Xu, M., 2022. Toxic effects of nanoplastics with different sizes and surface charges on epithelial-to-mesenchymal transition in A549 cells and the potential toxicological mechanism. J. Hazard Mater. 430, 128485 https://doi.org/10.1016/j.jhazmat.2022.128485.

Huang, J., Dong, G., Liang, M., Wu, X., Xian, M., An, Y., Zhan, J., Xu, L., Xu, J., Sun, W., Chen, S., Chen, C., Liu, T., 2022. Toxicity of micro(nano)plastics with different size and surface charge on human nasal epithelial cells and rats via intranasal exposure. Chemosphere 307 (Pt 4), 136093. https://doi.org/10.1016/j.chemosphere.2022.136093.

Ivleva, N.P., 2021. Chemical analysis of microplastics and nanoplastics: challenges, advanced methods, and perspectives. Chem. Rev. 121 (19), 11886–11936. https://doi.org/10.1021/acs.chemrev.1c00178.

Karakolis, E.G., Nguyen, B., You, J.B., Rochman, C.M., Sinton, D., 2019. Fluorescent dyes for visualizing microplastic particles and fibers in laboratory-based studies. Environ. Sci. Technol. Lett. 6, 334–340. https://doi.org/10.1021/acs.estlett.9b00241.

Kik, K., Bukowska, B., Sicińska, P., 2020. Polystyrene nanoparticles: sources, occurrence in the environment, distribution in tissues, accumulation, and toxicity to various organisms. Environ. Pollut. 262. https://doi.org/10.1016/j.envpol.2020.114297.

Kim, S.A., Kim, L., Kim, T.H., An, Y.J., 2022. Assessing the size-dependent effects of microplastics on zebrafish larvae through fish lateral line system and gut damage. Mar. Pollut. Bull. 185 (Pt A), 114279 https://doi.org/10.1016/j.marpolbul.2022.114279.

Lesniak, A., Salvati, A., Santos-Martinez, M.J., Radomski, M.W., Dawson, K.A., Åberg, C., 2013. Nanoparticle adhesion to the cell membrane and its effect on nanoparticle uptake efficiency. J. Am. Chem. Soc. 135 (4), 1438–1444. https://doi.org/10.1021/ja309812z.

Liu, S., Li, Y., Shang, L., Yin, J., Qian, Z., Chen, C., Yang, Y., 2022. Size-dependent neurotoxicity of micro- and nanoplastics in flowing condition based on an in vitro microfluidic study. Chemosphere 303 (Pt 3), 135280. https://doi.org/10.1016/j.chemosphere.2022.135280.

Mamun, A.A., Prasetya, T.A.E., Dewi, I.R., Ahmad, M., 2023. Microplastics in human food chains: food becoming a threat to health safety. Sci. Total Environ. 858 (Pt 1), 159834 https://doi.org/10.1016/j.scitotenv.2022.159834.

Nguyen, B., Tufenkji, N., 2022. Single-particle resolution fluorescence microscopy of nanoplastics. Environ. Sci. Technol. 56 (10), 6426–6435. https://doi.org/10.1021/acs.est.1c08480.

Qiao, R., Mortimer, M., Richter, J., Rani-Borges, B., Yu, Z., Heinlaan, M., Lin, S., Ivask, A., 2022. Hazard of polystyrene micro-and nanospheres to selected aquatic and terrestrial organisms. Sci. Total Environ. 853, 158560 https://doi.org/10.1016/j.scitotenv.2022.158560.

Ramsperger, A.F.R.M., Bergamaschi, E., Panizzolo, M., Fenoglio, I., Barbero, F., Peters, R., Undas, A., Purker, S., Giese, B., Lalyer, C.R., Tamargo, A., Moreno-Arribas, M.V., Grossart, H.P., Kühnel, D., Dietrich, J., Paulsen, F., Afanou, A.K., Zienolddiny-Narui, S., Eriksen Hammer, S., Kringlen Ervik, T., Graff, P., Brinchmann, B.C., Nordby, K.C., Wallin, H., Nassi, M., Benetti, F., Zanella, M., Brehm, J., Kress, H., Löder, M.G.J., 2022. Laforsch CNano- and microplastics: a comprehensive review on their exposure routes, translocation, and fate in humans. NanoImpact 29, 100441. https://doi.org/10.1016/j.impact.2022.100441.

Rubio, L., Marcos, R., Hernández, A., 2020a. Potential adverse health effects of ingested micro- and nanoplastics on humans. Lessons learned from in vivo and in vitro mammalian models. J. Toxicol. Environ. Health B Crit. Rev. 23 (2), 51–68. https://doi.org/10.1080/10937404.2019.1700598.

Rubio, L., Barguilla, I., Domenech, J., Marcos, R., Hernández, A., 2020b. Biological effects, including oxidative stress and genotoxic damage, of polystyrene nanoparticles in different human hematopoietic cell lines. J. Hazard Mater. 398, 22900 https://doi.org/10.1016/j.jhazmat.2020.122900.

Sawyer, L., Grubb, D.T., Meyers, G.F., 2008. Polymer Microscopy. Springer Science and Business Medium, New York. https://doi.org/10.1007/978-0-387-72628-1.

Shadel, G.S., Horvath, T.L., 2015. Mitochondrial ROS signaling in organismal homeostasis. Cell 163, 560–569. https://doi.org/10.1016/j.cell.2015.10.001.

Tenuta, T., Monopoli, M.P., Kim, J., Salvati, A., Dawson, K.A., Sandin, P., Lynch, I., 2011. Elution of labile fluorescent dye from nanoparticles during biological use. PLoS One 6 (10), e25556. https://doi.org/10.1371/journal.pone.0025556.

Tursi, A., Baratta, M., Easton, T., Chatzisymeon, E., Chidichimo, F., De Biase, M., De Filpo, G., 2022. Microplastics in aquatic systems, a comprehensive review: origination, accumulation, impact, and removal technologies. RSC Adv. 12 (44), 28318–28340. https://doi.org/10.1039/d2ra04713f.

Wang, Q., Bai, J., Ning, B., Fan, L., Sun, T., Fang, Y., Wu, J., Li, S., Duan, C., Zhang, Y., Liang, J., Gao, Z., 2020. Effects of bisphenol A and nanoscale and microscale polystyrene plastic exposure on particle uptake and toxicity in human Caco-2 cells. Chemosphere 254, 126788. https://doi.org/10.1016/j.chemosphere.2020.126788.

Wu, B., Wu, X., Liu, S., Wang, Z., Chen, L., 2019. Size-dependent effects of polystyrene microplastics on cytotoxicity and efflux pump inhibition in human Caco-2 cells. Chemosphere 221, 333–341. https://doi.org/10.1016/j.chemosphere.2019.01.056.

Wu, Y., Yao, Y., Bai, H., Shimizu, K., Li, R., Zhang, C., 2023. Investigation of pulmonary toxicity evaluation on mice exposed to polystyrene nanoplastics: the potential protective role of the antioxidant N-acetylcysteine. Sci. Total Environ., 158851 https://doi.org/10.1016/j.scitotenv.2022.158851, 855.

Xu, M., Halimu, G., Zhang, Q., Song, Y., Fu, X., Li, Y., Li, Y., Zhang, H., 2019. Internalization and toxicity: a preliminary study of effects of nanoplastic particles on human lung epithelial cell. Sci. Total Environ. 694, 133794 https://doi.org/10.1016/j.scitotenv.2019.133794.

Xu, C., Zhang, B., Gu, C., Shen, C., Yin, S., Aamir, M., Li, F., 2020. Are we underestimating the sources of microplastic pollution in terrestrial environment? J. Hazard Mater. 400, 123228 https://doi.org/10.1016/j.jhazmat.2020.123228.

Yang, S., Cheng, Y., Chen, Z., Liu, T., Yin, L., Pu, Y., Liang, G., 2021. *In vitro* evaluation of nanoplastics using human lung epithelial cells, microarray analysis and co-culture model. Ecotoxicol. Environ. Saf. 226, 112837 https://doi.org/10.1016/j.ecoenv.2021.112837.

Yong, C.Q.Y., Valiyaveettil, S., Tang, B.L., 2020. Toxicity of microplastics and nanoplastics in mammalian systems. Int. J. Environ. Res. Publ. Health 17 (5), 1509. https://doi.org/10.3390/ijerph17051509.

Zhang, Y.X., Wang, M., Yang, L., Pan, K., Miao, A.J., 2022. Bioaccumulation of differently sized polystyrene nanoplastics by human lung and intestine cells. J. Hazard Mater. 439, 129585 https://doi.org/10.1016/j.jhazmat.2022.129585.

Zhou, N., Wang, Z., Yang, L., Zhou, W., Qin, Z., Zhang, H., 2023. Size-dependent toxicological effects of polystyrene microplastics in the shrimp *Litopenaeus vannamei* using a histomorphology, microbiome, and metabolic approach. Environ. Pollut. 316 (Pt 2), 120635 https://doi.org/10.1016/j.envpol.2022.120635.